Observational Determination of the Gravitational Potential and Pattern Speed in Strongly Barred Galaxies

Per A.B. Lindblad and Per Olof Lindblad

Stockholm Observatory, AlbaNova, SE–10691 Stockholm, Sweden

Abstract. In order to compute stellar orbits in spiral galaxies the gravitational potential and its pattern speed must be known. Observationally, these parameters are difficult to determine, in particular for strongly barred galaxies. We will briefly review different methods and illustrate in more detail the case where the problem has been approached by numerical gasdynamical simulations.

1 Introduction

When computing orbits in real galaxies one needs to know the gravitational potential and its pattern speed, i.e. the angular velocity of its non-axisymmetric component. In the quasi-steady density wave picture of galaxy dynamics these two quantities are considered to be more or less constant throughout the system and over a certain period of time.

To derive the gravitational potential from photometry requires very accurate multicolour photometry to very faint levels with corrections for extinction and assuming mass-luminosity ratios for a mixture of stellar populations. To this must be added the potential of an unknown amount of dark matter. Where the symmetry plane of the galaxy is suitably inclined to the plane of the sky, radial velocities will give information of the kinematics in the plane of the galaxy, complementing the information from photometry.

The axisymmetric part of the potential in the plane of the galaxy is generally described by the rotation curve, whereby we mean the set of circular orbital velocities as a function of the distance from the centre, given by the axisymmetric Fourier component of the density distribution.

The interplay between the orbital motions and the pattern speed gives rise to various resonance phenomena, of which we in particular note the corotation resonance (CR) and the Inner (ILR) and Outer (OLR) Lindblad Resonances. The CR occurs where the orbital angular velocity is close to the pattern speed. Any regular non-circular particle orbit can be described as a closed orbit with n pericentra, rotating with a certain angular velocity. The rotation can be slower than the mean orbital velocity, so that the particle describes the rotating closed orbit mainly in the forward direction, or faster, so that the particle describes the closed orbit mainly in the retrograde direction. Where the rotation of the orbit, for $n = 2$, is close to the pattern speed, we have an ILR in the former case and an OLR in the latter. For one and the same pattern ILR and OLR fall on different sides of CR. There remains the possibility that one and the same system may contain different structural components each with its own pattern speed [10].

In the case of a weak bar with small deviations from circular motion we have a circular corotation region, where the circular angular velocity is close to the pattern speed. This case is well demonstrated by England, Hunter and Contopoulos [2] by hydrodynamical model computations of motions in various bar potentials. Figure 1 shows the case of a rather weak bar perturbation. To the left is shown the gas density response pattern when the gas has been settled into a quasi-steady state, and to the right the gas velocity vectors in a frame rotating with the pattern.

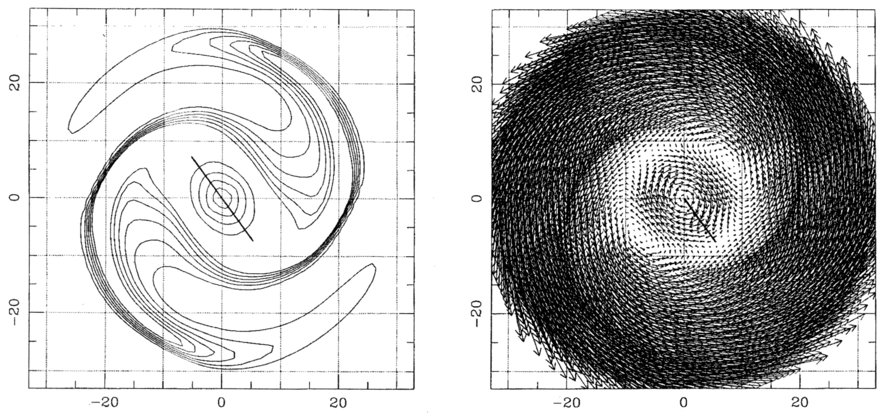

Fig. 1. Gas density response (left) and velocity vectors (right) of a rotating bar perturbation of moderate strength. The system rotates clock-wise. A straight line in the figures shows the position and extent of the bar. From [2]

The circular corotation region of low velocities is clearly seen in this figure. It contains two vortex regions, corresponding to the Lagrangian L4 and L5 equilibrium points of the restricted 3-body problem. In these regions the gas rotates counter clock-wise and expands from the vortex centre.

The case of a very strong bar, as shown in Fig. 2, however, is different. In the bar region there is no continuous set of nearly circular orbits and no circle of corotation resonance. Here the corotation region has broken down. There are still the two vortices placed at right angels to the bar, now very pronounced. In addition, there are two vortices close to the gas density maxima in the bar, around which the gas now flows in the same direction as the bar rotation and inwards towards the vortex centre. There also seem to be low velocity corotation regions outside the ends of the bar. The entire bar is close to corotating.

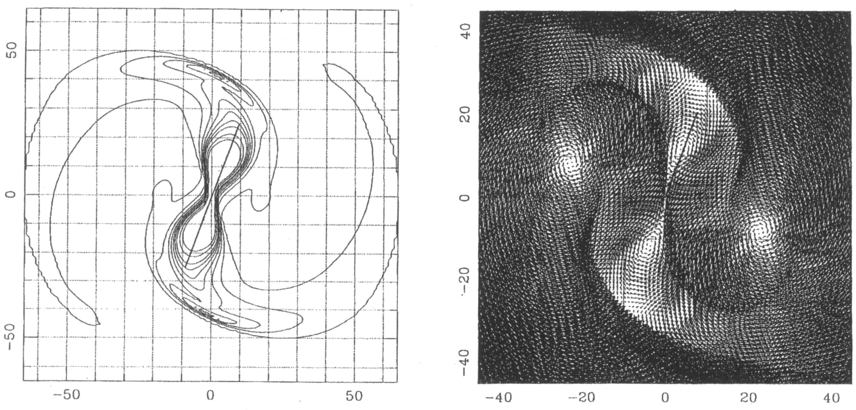

Fig. 2. Gas density response (left) and velocity vectors (right) of a rotating very strong bar perturbation. The system rotates clock-wise. A straight line in the figures shows the position and extent of the bar. From [2]

To derive a rotation curve in the bar region from the observed radial velocities in such a galaxy would be a very difficult task and its usefulness might be questioned.

2 Methods to determine the pattern speed

A sophisticated scheme to derive the pattern speed for a non-circular-symmetric pattern in open spiral and barred galaxies was suggested by Tremaine and Weinberg [11]. The scheme is based on the continuity equation and is rather model independent. It is assumed that the disk has a well defined pattern speed, that the surface brightness of the tracer obeys the continuity equation, and that there is no streaming velocity normal to the disk plane.

The continuity equation is integrated over a strip parallel to the apparent major axis of the system. The gain and loss of matter across the strip, due to the rotation of the pattern, is related to the radial velocities and luminosity distribution along the strip.

Figure 3 illustrates the version of this method designed by Merrifield and Kuijken [9], here applied to the early type SB galaxy NGC 4596 [3]. The spectra are added all along the slit, and the right side shows the Doppler broadening function of this single absorption line spectrum determined by means of a templet star. This is done for three different slit offsets along the minor axis. On the bottom we see the continuum luminosity distribution along the same slits. Each pair gives a point in the diagram. The slope of the line is proportional to the pattern speed multiplied with the sin i of the inclination of the plane of the galaxy to the plane of the sky. This can be extended to any number of slits.

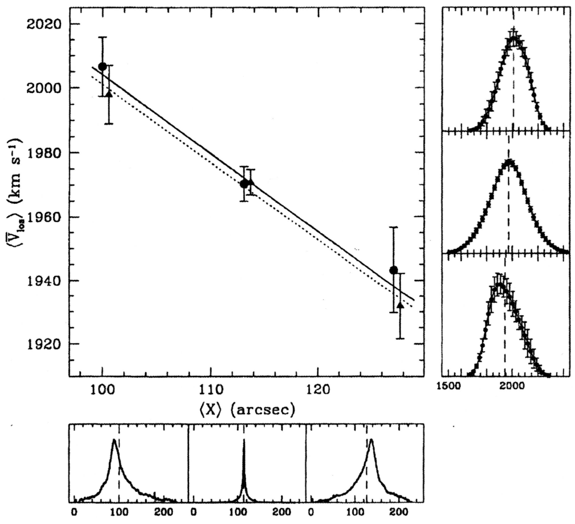

Fig. 3. Mean line-of-sight velocities versus luminosity centroid position for three slits parallel to the major axis of NGC 4596. From [3]

The method has been applied to a handful of early type barred galaxies. Its potential usefulness, however, for H I observations in barred galaxies is doubtful. Figure 4 shows an optical image as well as the total neutral hydrogen map of the barred galaxy NGC 1365. Typically, H I disappears in the bar region, where the deviation from circular symmetry is the largest and the method is most useful. The continuity equation is not valid. In the spiral arms H I is forming stars and along the bar H I is transferred to molecular hydrogen streaming towards the centre. Our efforts have shown that the method cannot be meaningfully applied to the H I data for NGC 1365.

Several authors have tried to identify the positions of a corotation circle, or other specific resonances, in real galaxies and from the rotation curve get the pattern speed. In some cases this procedure seems to start from assumptions that should be proven in the end.

A method, based on the linear density wave theory, has been suggested by Canzian [1]. According to this theory the residual radial velocities along the line of sight, when the rotation curve has been subtracted, should be proportional to $\sin \Phi$ close to the ILR, where Φ is the central angle in the plane of the galaxy, and proportional to $\sin 3\Phi$ close to the OLR. At corotation the amplitudes of the two functions should have a specific ratio, dependent of the shape of the rotation curve. The method is very sensitive to the proper derivation of the rotation curve and the residual velocities. Being based on the linear density wave theory it should not be applicable to barred spirals.

If there is no easy way out, the ultimate method is to make a simulation of the entire galaxy, taking into consideration all available observational information. Several authors have done this in different ways. In the course of such a simulation procedure one should get a rotation curve, perturbing potential and pattern speed, consistent with the observed velocity field and giving resonance regions compatible with the observed morphology.

3 The case of NGC 1365

To illustrate the procedure, let us consider the case of NGC 1365 which was simulated by Per A.B. Lindblad in a project at Stockholm Observatory, in which we collaborated with E. Athanassoula in Marseille [5]. A similar analysis has been performed, among others, by Weiner, Sellwood, Williams, and van Gorkom in the case of the SB galaxy NGC 4123 [13] [12], using the same gasdynamical code.

NGC 1365 (Fig. 4) is one of the more thoroughly studied nearby isolated barred galaxies [6]. Its inclination to the plane of the sky of 40° is suitable for radial velocity studies of the kinematics, and the inclination of the bar to the line of nodes close to optimal for a study of streaming both across and along the bar. The distance is 18 Mpc, which gives a scale where $1''$ corresponds to 100 pc. With a diameter of $11'$, or 66 kpc, it is a supergiant galaxy.

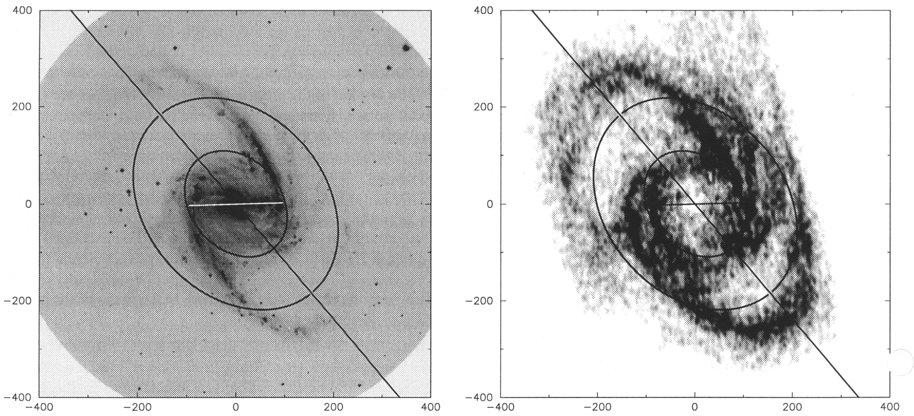

Fig. 4. An optical ESO 3.6 m prime focus plate (left) and total H I column density map (right) of NGC 1365. The ellipses enclose the region where the rotation curve is believed to give a reliable description of the axisymmetric forces. The bar major axis and the line of nodes are marked as straight lines running through the centre. From [5]

Detailed VLA observations in H I have been presented by Jörsäter and van Moorsel [4]. The total H I density map is given in Fig. 4. As was mentioned, H I is very scarce in the bar region. In the very nucleus H I is seen in absorption.

However, the central region was filled in with velocities from long slit emission line spectra, and a complete radial velocity map for the interstellar gas was constructed [7]. In Fig. 5 we see the characteristic twist along the bar and wiggles along spiral arms.

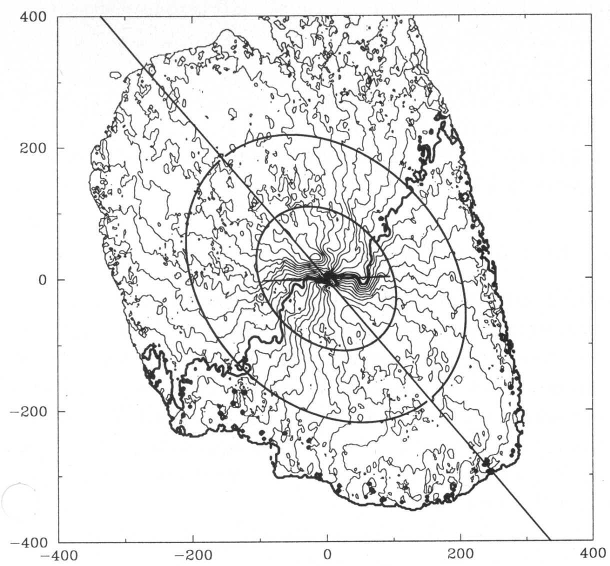

Fig. 5. The observed radial velocity field of NGC 1365. The contour interval is 20 km/s, and the systemic velocity is drawn as a thick line. The ellipses are the same as in Fig. 4. From [5]

In Figs. 4 and 5 the ellipses separate the *bar region*, *intermediate region* and *outer region*. As the basis for the rotation curve we adopt the azimuthally averaged rotation curve of Jörsäter and van Moorsel. However, in the bar region such an azimuthally averaging method does not give a good approximation to the rotation curve, and in the outer region the system is warped, as seen from the kinematics in Fig. 5, which again makes the rotation curve uncertain.

To estimate the perturbing potential, we use infrared photometry, as the bar region shows a multitude of dust. We choose an infrared J-band image obtained as part of the Ohio-State University Bright Galaxy Imaging Survey (Fig. 6). This image was analysed in terms of even azimuthal Fourier components. As the spiral arms seem firmly attached to the ends of the bar, we assume that the spiral part of the structure, at least for a considerable time, has the same pattern speed as the bar.

At the start of the fitting procedure we let the axisymmetric part of the potential be represented by the Jörsäter–van Moorsel rotation curve. The perturbing potential is derived from the infrared surface photometry, where the

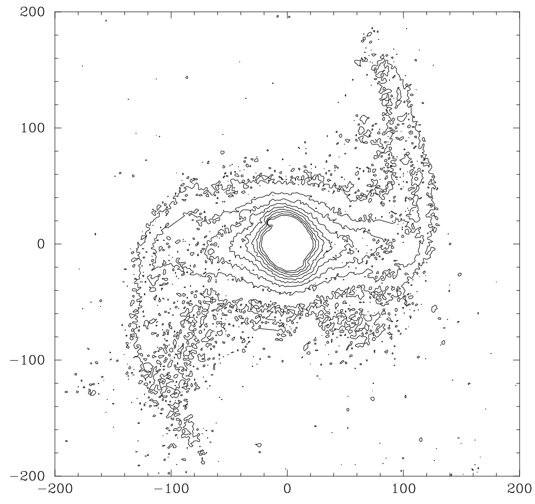

Fig. 6. Inclination corrected J-band image of NGC 1365. From [5]

mass/luminosity ratio M/L (in arbitrary units, as the photometry is not absolutely calibrated) is kept as a free parameter. This free parameter also compensates for effects of the unknown thickness of the bar.

The model fit in the intermediate region is rather insensitive to the exact shape of the rotation curve in the bar region. Thus, we can now make simulations with a sequence of different pattern speeds and M/L ratios to get the best fit to the structure in the *intermediate region.* The detailed structure in this region is particularly sensitive to the choice of pattern speed, and this speed can now be fixed to within a few km s^{-1} kpc^{-1}, at a value of 18 km s^{-1} kpc^{-1} for NGC 1365.

With the chosen value for the pattern speed we now adjust the Jörsäter–van Moorsel rotation curve in the *bar region* as well as the final choice of the perturbing M/L ratio, until the simulation reproduces the observed radial velocities from slit spectra as well as the morphology of the dust lanes along the bar, both of which lay constraints on the position of the ILR.

The result is seen in Fig. 7, where density contours of the model are overlaid the H I total column density map. The slight mismatch in the outer region is due to the steep decline of the Jörsäter–van Moorsel rotation curve. If raised about 10 km/s in the outer region, the OLR and spiral arms move outward (i.e. a less drastic warp is assumed) and the match is improved.

Figure 8 compares the observed radial velocity field with that given by the model as observed from the same angle. The forced bisymmetry of the model limits the fit in both Figs. 7 and 8. In spite of this, the main features are reproduced fairly well. The velocity pattern in Fig. 8 shows the characteristics of orbits elongated along the bar. The shocks along the bar are smoothed in frame

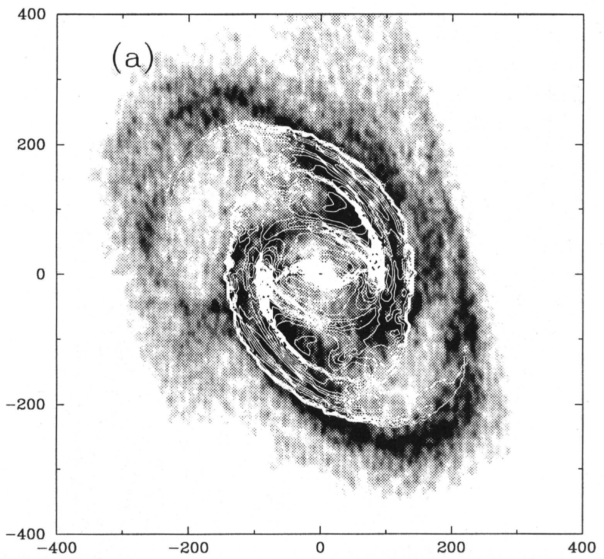

Fig. 7. Model density contours overlaid the total column H I density map. From [5]

(**a**) due to the procedure with which the velocity field was constructed from randomly positioned slits. Thus, here a comparison should be made directly with slit measurements. Figure 9 shows this for a slit placed perpendicular to the bar 29″ East of the nucleus. The jump across the shock of 300 km/s is well reproduced.

Thus, we arrive at a possible variation of the axisymmetric forces and a pattern speed which are in agreement with the observed morphology and velocity field. In contrast, Weiner et al. [12] through accurate photometry and by the perturbations required, assuming the same M/L for disk and bar, derive by simulations similar to ours this M/L and deduce the mass of the halo required to reproduce the outer rotation curve. This means that they use the perturbations from the bar to infer a M/L for the disk and bar and get the mass of the dark halo component. For NGC 1365 this would not be safe due to the warp, which makes the outer rotation curve uncertain.

The gas flow in a frame rotating with the pattern is shown in Fig. 10, where the circles mark the ILR, CR and OLR resonance positions. Only half of the velocity field is shown. The orbits show the familiar twist around the ILR [8] as well as the change of direction of the flow at the shock fronts along the bar. The spiral arms extending from the ends of the bar appear also for a purely barred perturbation, but the spiral part of the potential is necessary to drive the arms through corotation. The vortex regions at CR are apparent.

Thus, through detailed comparison between observations and models, estimates of the pattern speed as well as total gravitational potential can be obtained

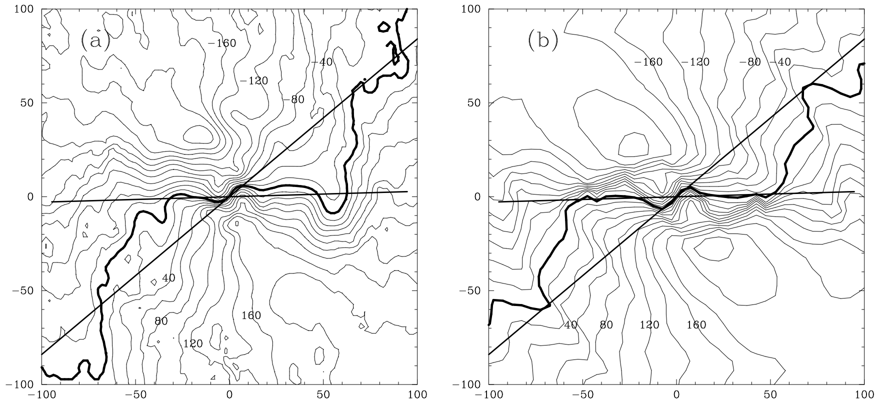

Fig. 8. Comparison between the observed velocity field in NGC 1365 (**a**) and that given by the model (**b**). The orientations of the bar axis in PA 92° and the minor axis of the galaxy in PA 130° are shown as straight lines. From [5]

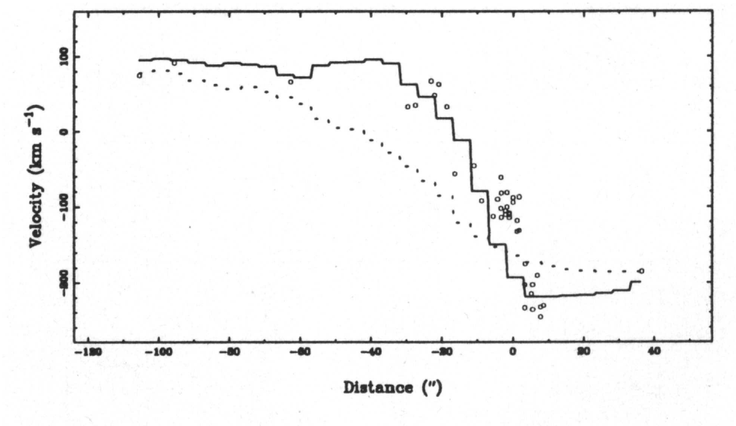

Fig. 9. Radial velocities along a slit placed perpendicular to the bar 29″ East of the nucleus. Open circles: observed velocities. Solid line: model velocities. Dotted line: pure rotational motion according to the rotation curve. From [5]

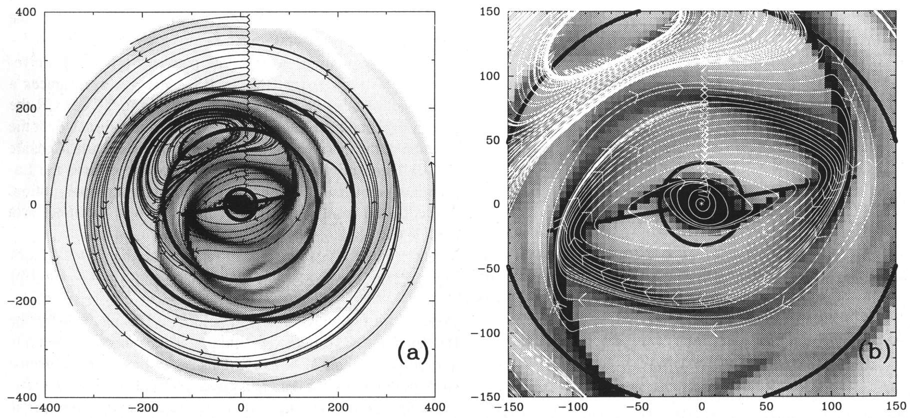

Fig. 10. Gas flow lines from the model overlaid gray scale maps of the same model. Full scale (**a**), bar region (**b**). From [5]

for individual galaxies. This will permit us to compute stellar orbits in rather realistic, but in our case bi-symmetrical, galaxy potentials.

References

1. B. Canzian: Astrophys. J. **414**, 487 (1993)
2. M.N. England, J.H. Hunter Jr., G. Contopoulos: Astrophys. J. **540**, 154 (2000)
3. J. Gerssen, K. Kuiken, M.R. Merrifield: Month. Not. Roy. Astr. Soc. **306**, 926 (1999)
4. S. Jörsäter, G. van Moorsel: Astron. J. **110**, 2037 (1995)
5. P.A.B. Lindblad, P.O. Lindblad, E. Athanassoula: Astron. Astrophys. **313**, 65 (1996)
6. P.O. Lindblad: Astron. Astrophys. Rev. **9**, 221 (1999)
7. P.O. Lindblad, M. Hjelm, J. Högbom, S. Jörsäter, P.A.B. Lindblad, M. Santos-Lleó: Astron. Astrophys. Suppl. **120**, 403 (1996)
8. P.O. Lindblad, P.A.B. Lindblad: Publ. Astr. Soc. Pacific Conf. **66**, 29 (1994)
9. M.R. Merrifield, K. Kuijken: Month. Not. Roy. Astr. Soc. **274**, 933 (1995)
10. J.A. Sellwood, L.S. Sparke: Month. Not. Roy. Astr. Soc. **231**, 25p (1988)
11. S. Tremaine, M.D. Weinberg: Astrophys. J. **282**, L5 (1984)
12. B.J. Weiner, J.A. Sellwood, T.B. Williams: Astrophys. J. **546**, 931 (2001)
13. B.J. Weiner, T.B. Williams, J.H. van Gorkom, J.A. Sellwood: Astrophys. J. **546**, 916 (2001)